



Contents lists available at ScienceDirect

## Journal of the Mechanics and Physics of Solids

journal homepage: [www.elsevier.com/locate/jmps](http://www.elsevier.com/locate/jmps)

# Merging mechanical and electromechanical bandgaps in locally resonant metamaterials and metastructures

C. Sugino<sup>a</sup>, M. Ruzzene<sup>a,b</sup>, A. Erturk<sup>a,\*</sup><sup>a</sup> G.W. Woodruff School of Mechanical Engineering, Georgia Institute of Technology, Atlanta, GA, USA<sup>b</sup> D. Guggenheim School of Aerospace Engineering, Georgia Institute of Technology, Atlanta, GA, USA

## ARTICLE INFO

## Article history:

Received 1 August 2017

Revised 9 April 2018

Accepted 10 April 2018

Available online 12 April 2018

## Keywords:

Metamaterial

Metastructure

Locally resonant

Bandgap

Hybrid

## ABSTRACT

Locally resonant metamaterials are characterized by bandgaps at wavelengths much larger than the lattice size. Such locally resonant bandgaps can be formed using mechanical or electromechanical resonators. However, the nature of bandgap formation in mechanical and electromechanical (particularly piezoelectric) metamaterials is fundamentally different since the former is associated with a dynamic modal mass, while the latter is due to a dynamic modal stiffness. Next-generation metamaterials and resulting metastructures (i.e. finite configurations with specified boundary conditions) hosting mechanical resonators as well as piezoelectric interfaces connected to resonating circuits can enable the formation of two bandgaps, right above and below the design frequency of the mechanical and electrical resonators, respectively, yielding a wider bandgap and enhanced design flexibility as compared to using a purely mechanical, or a purely electromechanical configuration. In this work, we establish a fully coupled framework for hybrid mechanical-electromechanical metamaterials and finite metastructures. Combined bandgap size is approximated in closed form as a function of the added mass ratio of the resonators and the system-level electromechanical coupling for the infinite resonators approximation. Case studies are presented for a hybrid metamaterial cantilever under bending vibration to understand the interaction of these two locally resonant metamaterial domains in bandgap formation. Specifically, it is shown that the mechanical and electromechanical bandgaps do not fully merge for a finite number of resonators in an undamped setting. However, the presence of even light damping in the resonators suppresses the intermediate resonances emerging within the combined bandgap, enabling seamless merging of the two bandgaps in real-world structures that have damping. The overall concept of combining mechanical and electromechanical bandgaps in the same single metastructure can be leveraged in more complex topologies of piezoelectric metamaterial-based solids and structures.

© 2018 Elsevier Ltd. All rights reserved.

## 1. Introduction

The research domain of acoustic/elastic metamaterials has lately received growing attention (Chen et al., 2017; Dong et al., 2017; Krushynska et al., 2014; Liu et al., 2015; 2000; Sugino et al., 2016; 2017b). Among the remarkable properties offered by various metamaterial concepts, in particular, locally resonant metamaterials (Liu et al., 2000) yield bandgap for-

\* Corresponding author.

E-mail address: [alper.erturk@me.gatech.edu](mailto:alper.erturk@me.gatech.edu) (A. Erturk).

mation at wavelengths much larger than the lattice size of the host structure, enabling low-frequency vibration and sound attenuation. In their seminal work, Liu et al. (2000) first demonstrated this behavior using hard metal spheres embedded in a soft rubber as mechanical resonators. Other researchers have considered purely mechanical locally resonant metamaterials of various types (Baravelli and Ruzzene, 2013; Matlack et al., 2016; Nouh et al., 2015; Oudich et al., 2011; Wang et al., 2014; Yang et al., 2008; Zhu et al., 2014), using a variety of methods, such as the plane wave expansion method, transfer matrix method, or finite element method. These unit-cell based dispersion techniques lose information regarding the boundary conditions and mode shapes of the finite-size structure (i.e. metamaterial-based finite metastructure). To this end, we recently established and experimentally validated a modal analysis approach to derive the edge frequencies of the mechanical locally resonant bandgap in closed form (Sugino et al., 2016; 2017b), in addition to quantifying the number of resonators required in a finite structure for bandgap formation and understanding the effect of non-uniform resonator distribution. Specifically, the bandgap size (Sugino et al., 2016; 2017b) depends on the total added mass ratio provided that a sufficient number of resonators exist.

In another body of work (Airoidi and Ruzzene, 2011; Bergamini et al., 2015; Casadei et al., 2010; Jin et al., 2014; Senesi and Ruzzene, 2011; Sugino et al., 2017a), the use of piezoelectric elements shunted to resonating circuits (Hagood and von Flotow, 1991; Lesieutre, 1998) has lately been explored for locally resonant bandgap formation. These electromechanical resonators have the benefit of significantly lower mass requirements than purely mechanical mass-spring resonators. When many of these electromechanical resonators are placed on a structure, in analogy with a purely mechanical locally resonant metastructure, the structure can exhibit an electromechanical locally resonant bandgap (Airoidi and Ruzzene, 2011; Bergamini et al., 2015; Casadei et al., 2010; Jin et al., 2014; Senesi and Ruzzene, 2011; Sugino et al., 2017a). Recently (Sugino et al., 2017a), we used modal analysis to derive the edge frequencies of the locally resonant bandgap for a piezoelectric bimorph beam, finding that the shunt circuitry adds frequency-dependence to the dynamic stiffness of each mode of the structure. As a result, the purely piezoelectric locally resonant bandgap size mainly depends on the system level electromechanical coupling (Sugino et al., 2017a), e.g. single crystal piezoelectric materials yield larger bandgap than piezoelectric ceramics.

Since the phenomena responsible for the mechanical and electromechanical locally resonant bandgaps are fundamentally different (i.e. negative dynamic mass vs. negative dynamic stiffness), the two types of behavior can be combined in a single, hybrid metastructure. Here we consider a representative hybrid metastructure (a piezoelectric bimorph cantilever with segmented electrodes shunted to resonant circuits and mechanical resonators undergoing bending vibrations) to show that the two bandgaps can be combined into a single, larger bandgap for increased bandwidth, or that the two bandgaps can be placed separately for increased flexibility to tailor the frequency response. Numerical case studies are presented and results from modal analysis are compared with the dispersion curves obtained using the plane wave expansion method.

## 2. Hybrid piezoelectric metamaterial beam with mechanical and electromechanical resonators

Consider a piezoelectric bimorph beam with rectangular cross section made from two continuous piezoelectric layers sandwiching a central shim, with the piezoelectric layers poled in opposite transverse directions (i.e. series connection under bending vibration). The outer surface electrodes are segmented as pairs and connected to a total of  $S$  shunt circuits, which span a region  $x_j^L < x < x_j^R$ , where  $j = 1 \dots S$  is an index numbering the shunt circuits, and  $x_j^L$  and  $x_j^R$  are the left and right ends of the  $j$ th pair of electrodes, respectively. The purely piezoelectric problem was considered by Sugino et al. (2017a), but here we introduce mechanical locally resonant metastructure performance by adding  $S$  mechanical resonators to the structure at the right end of each electrode, i.e. at  $x = x_j^R$ . A schematic of the system is shown in Fig. 1 in the absence of external forcing.

The governing equations for the bimorph, resonators, and shunt circuits can be obtained as

$$EI \frac{\partial^4 w}{\partial x^4} + m \frac{\partial^2 w}{\partial t^2} - \sum_{j=1}^S k_j u_j(t) \delta(x - x_j^R) - \vartheta \sum_{j=1}^S v_j(t) \frac{\partial^2}{\partial x^2} [H(x - x_j^L) - H(x - x_j^R)] = f(x, t) \quad (1)$$

$$m_j \ddot{u}_j + k_j u_j(t) + m_j \ddot{w}(x_j^R, t) = 0 \quad (2)$$

$$C_{p,j} \dot{v}_j(t) + \mathcal{Y}_j[v_j(t)] + \vartheta \int_{x_j^L}^{x_j^R} \frac{\partial^3 w}{\partial x^2 \partial t} dx = 0 \quad (3)$$

where  $w(x, t)$  is the transverse displacement of the beam,  $k_j$  is the stiffness of the  $j$ th resonator,  $u_j(t)$  is the displacement of the  $j$ th resonator,  $v_j(t)$  is the voltage across the  $j$ th pair of electrodes,  $\mathcal{Y}_j$  is a linear integro-differential operator corresponding to the admittance of the  $j$ th shunt circuit,  $H(x)$  is the Heaviside function, and  $f(x, t)$  is the external forcing. While

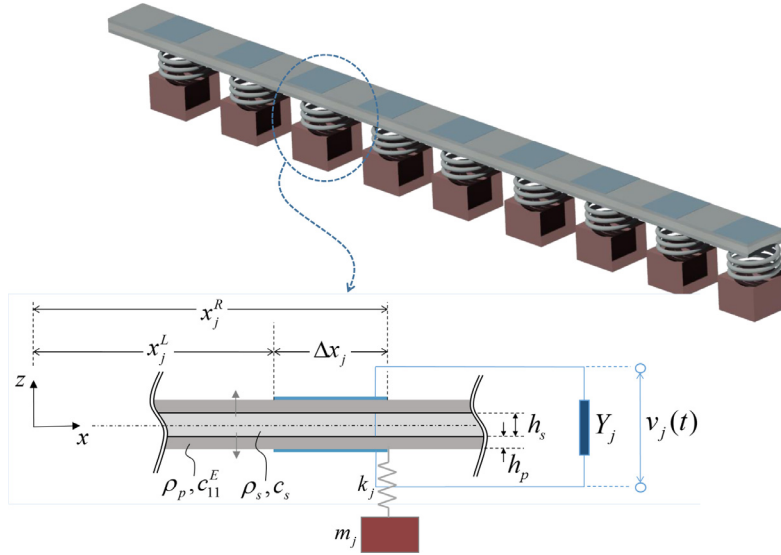


**Fig. 1.** Schematic of the combined mechanical-electromechanical metastructure. The piezoelectric bimorph beam has segmented electrode pairs shunted to resonating circuits, with a mechanical resonator placed at the right end of each electrode.

the governing equations are undamped, modal damping or resonator damping can easily be added at a later stage. The locally resonant bandgap phenomenon is most simply derived in the absence of any damping, without loss of generality. The effective properties of the bimorph are

$$EI = \frac{2b}{3} \left( c_s \frac{h_s^3}{8} + \bar{c}_{11}^E \left[ \left( h_p + \frac{h_s}{2} \right)^3 - \frac{h_s^3}{8} \right] \right) \tag{4}$$

$$m = b(\rho_s h_s + 2\rho_p h_p) \tag{5}$$

$$\vartheta = \frac{\bar{e}_{31} b_e}{2h_p} \left[ \left( h_p + \frac{h_s}{2} \right)^2 - \frac{h_s^2}{4} \right] \tag{6}$$

$$C_{p,j} = \frac{\bar{\varepsilon}_{33}^S b_e \Delta x_j}{2h_p} \tag{7}$$

The parameters  $c_s$ ,  $\rho_s$ , and  $h_s$  are the central substrate layer’s elastic modulus, mass density, and thickness, respectively, while  $b$  is the width of the beam. The piezoelectric layers have mass density  $\rho_p$ , thickness  $h_p$ , width  $b$ , elastic modulus at constant electric field  $\bar{c}_{11}^E$ , effective piezoelectric stress constant  $\bar{e}_{31}$ , and permittivity component at constant strain  $\bar{\varepsilon}_{33}^S$ , where the overbars indicate effective properties for 1D thin layers reduced from the full 3D constitutive equations, defined as

$$\bar{c}_{11}^E = \frac{1}{s_{11}^E}, \quad \bar{e}_{31} = \frac{d_{31}}{s_{11}^E}, \quad \bar{\varepsilon}_{33}^S = \varepsilon_{33}^T - \frac{d_{31}^2}{s_{11}^E} \tag{8}$$

where  $s_{11}^E$  is the elastic compliance at constant electric field,  $d_{31}$  is the piezoelectric strain constant, and  $\varepsilon_{33}^T$  is the permittivity component at constant stress. We assume a modal expansion for  $w(x, t)$ , i.e.

$$w(x, t) = \sum_{r=1}^N \phi_r(x) \eta_r(t) \tag{9}$$

where  $\phi_r(x)$  are the mass-normalized mode shapes of the structure without resonators (i.e. the plain structure) at short circuit,  $\eta_r(t)$  are the modal coordinates to be determined, and  $N$  is number of modes used in the expansion. The mass-normalized mode shapes of the plain structure at short circuit satisfy the orthogonality conditions

$$\int_0^L m \phi_r(x) \phi_k(x) dx = \delta_{rk} \tag{10}$$

$$\int_0^L EI\phi_r(x) \frac{d^4\phi_k}{dx^4} dx = \omega_r^2 \delta_{rk} \quad (11)$$

where  $\omega_r^2$  is the  $r$ th squared natural frequency of the plain structure at short circuit and  $\delta_{rs}$  is the Kronecker delta. Substituting Eq. (9) into Eq. (1), multiplying by another mode shape  $\phi_k(x)$ , and applying the orthogonality conditions Eqs. (10) and (11) gives

$$\begin{aligned} \ddot{\eta}_r(t) + \omega_r^2 \eta_r(t) + \sum_{j=1}^S m_j \phi_r(x_j^R) \sum_{k=1}^N \ddot{\eta}_k(t) \phi_k(x_j^R) \\ + \sum_{j=1}^S m_j \ddot{u}_j(t) \phi_r(x_j^R) - \vartheta \sum_{j=1}^S v_j(t) \Delta\phi'_{r,j} = q_r(t) \end{aligned} \quad (12)$$

where  $\Delta\phi'_{r,j}$  is a slope difference defined as

$$\Delta\phi'_{r,j} = \left( \frac{d\phi_r}{dx} \right)_{x_j^R} - \frac{d\phi_r}{dx}(x_j^L) \quad (13)$$

and

$$q_r(t) = \int_0^L f(x, t) \phi_r(x) dx \quad (14)$$

is the modal excitation. Substituting Eq. (9) into Eqs. (2) and (3) yields

$$m_j \ddot{u}_j(t) + k_j u_j(t) + m_j \sum_{k=1}^N \ddot{\eta}_k(t) \phi_k(x_j^R) = 0 \quad (15)$$

$$C_{p,j} \dot{v}_j(t) + \mathcal{B}_j[v_j(t)] + \vartheta \sum_{r=1}^N \ddot{\eta}_r(t) \Delta\phi'_{r,j} = 0 \quad (16)$$

For a finite number of modes and shunt circuits/resonators, Eqs. (12), (15), and (16) can be solved for the approximate mode shapes and resonant frequencies of the system, as well as the system response, using techniques such as matrix inversion or modal decomposition. For more analytical insight, we take the Laplace transforms of Eqs. (12), (15), and (16), substituting the resonator equation and voltage equation into the modal governing equation to obtain

$$\begin{aligned} (s^2 + \omega_r^2) H_r(s) + \mu \frac{s^2 \omega_t^2}{s^2 + \omega_m^2} \sum_{k=1}^N H_k(s) \sum_{j=1}^S m \phi_k(x_j^R) \phi_r(x_j^R) \Delta x_j \\ + \frac{\alpha s}{s + h(s)} \sum_{k=1}^N H_k(s) \sum_{j=1}^S EI \frac{\Delta\phi'_{r,j}}{\Delta x_j} \frac{\Delta\phi'_{k,j}}{\Delta x_j} \Delta x_j = Q_r(s) \end{aligned} \quad (17)$$

where  $H_r(s)$  and  $Q_r(s)$  are the Laplace transforms of  $\eta_r(t)$  and  $q_r(t)$  respectively,  $s$  is the Laplace domain complex variable,  $\omega_m^2 = k_j/m_j$  is the squared resonant frequency of every mechanical resonator,  $\alpha$  is a dimensionless parameter related to electromechanical coupling (Sugino et al., 2017a):

$$\alpha = \frac{2\vartheta^2 h_p}{EI \varepsilon_{33} b_e} \quad (18)$$

and  $h(s) = Y_j(s)/C_{p,j}$  is a normalized admittance, assumed to be the same for each pair of electrodes, where  $Y_j(s)$  is the Laplace transform of  $\mathcal{B}_j$ . Additionally, it has been assumed that  $m_j = \mu m \Delta x_j$ , where  $\mu$  is the added mass ratio, a dimensionless parameter equal to the ratio of the total resonator mass to the total mass of the original structure.

Eq. (17) forms a system of  $N + 2S$  linear equations that can be solved numerically for the response at an excitation frequency  $\omega$  by substituting  $s = j\omega$  and using Gaussian elimination or matrix inversion. However, we observe that as the number of electrodes becomes large, and as the electrodes become very small,

$$\sum_{j=1}^S m \phi_k(x_j^R) \phi_r(x_j^R) \Delta x_j \approx \int_0^L m \phi_r(x) \phi_k(x) dx = \delta_{rk} \quad (19)$$

$$\sum_{j=1}^S EI \frac{\Delta\phi'_{r,j}}{\Delta x_j} \frac{\Delta\phi'_{k,j}}{\Delta x_j} \Delta x_j \approx \int_0^L EI \frac{d^2\phi_r}{dx^2} \frac{d^2\phi_k}{dx^2} dx = \omega_r^2 \delta_{rk} \tag{20}$$

since the summations become Riemann sum approximations of the orthogonality conditions in Eqs. (10) and (11) (note that the above symmetric form of the latter orthogonality condition is obtained via integration by parts twice). These approximations are exact as the shunt circuits become infinitesimally long and as the number of shunt circuits approaches infinity. The two approximations will not converge at the same rate, since the function being integrated is different in each approximation. This difference in rate of convergence will be apparent in later numerical studies.

Under the assumptions of Eqs. (19) and (20), the system of equations in Eq. (17) becomes decoupled, allowing us to solve explicitly for  $H_r(s)$  as

$$H_r(s) = \frac{Q_r(s)}{s^2 \left( 1 + \frac{\mu\omega_m^2}{s^2 + \omega_m^2} \right) + \omega_r^2 \left( 1 + \frac{\alpha s}{s + h(s)} \right)} \tag{21}$$

From this analysis it is clear that the presence of infinitely many mechanical resonators on the structure gives rise to frequency-dependent modal mass, and that the presence of infinitely many electromechanical resonators (i.e. electrode pairs with shunt circuits) gives rise to frequency-dependent modal stiffness.

### 3. Hybrid locally resonant bandgap

Although the theoretical development permits any type of normalized admittance  $h(s)$ , here we consider only purely inductive shunting and the resulting locally resonant bandgap. For electromechanical resonators (inductive shunt circuits) tuned to some resonant frequency  $\omega_e$ , the normalized admittance is

$$h(s) = \frac{\omega_e^2}{s} \tag{22}$$

where  $\omega_e^2 = 1/(L_j C_{p,j})$ , where  $L_j$  is the inductance applied to the  $j$ th shunt circuit. The resulting form of  $H_r(s)$  is

$$H_r(s) = \frac{Q_r(s)}{s^2 \left( 1 + \frac{\mu\omega_m^2}{s^2 + \omega_m^2} \right) + \omega_r^2 \left( 1 + \frac{\alpha s^2}{s^2 + \omega_e^2} \right)} \tag{23}$$

We can obtain the resonant frequencies explicitly by assuming an excitation frequency  $\omega$ , substituting  $s = j\omega$ , and solving for the roots of the polynomial in the denominator. However, the resulting expressions are complex and not useful for design purposes. Instead, it is simpler to consider the effective dynamic mass and stiffness of the system, i.e.

$$\frac{H_r(j\omega)}{Q_r(j\omega)} = \frac{1}{K(j\omega)\omega_r^2 - M(j\omega)\omega^2} \tag{24}$$

where

$$M(j\omega) = 1 + \frac{\mu\omega_m^2}{\omega_m^2 - \omega^2}, \quad K(j\omega) = 1 - \frac{\alpha\omega^2}{\omega_e^2 - \omega^2} \tag{25}$$

There can only be positive real roots in the denominator of Eq. (24) for  $\omega$  when both  $K(j\omega)$  and  $M(j\omega)$  have the same sign. We can see from Eq. (25) that the dynamic mass  $M(j\omega)$  is negative for

$$\omega_m < \omega < \omega_m \sqrt{1 + \mu} \tag{26}$$

and positive otherwise, whereas the dynamic stiffness  $K(j\omega)$  is negative for

$$\frac{\omega_e}{\sqrt{1 + \alpha}} < \omega < \omega_e \tag{27}$$

and positive otherwise. We expect a locally resonant bandgap in frequency ranges where  $M(j\omega)$  and  $K(j\omega)$  have opposite signs, since there can be no resonant frequencies. Furthermore, since both the terms in the denominator in Eq. (24) will have the same sign, the resulting amplitude of  $H_r(j\omega)$  will be small, resulting in significant vibration attenuation. If the two frequency ranges in Eqs. (26) and (27) are distinct, each will correspond to a separate locally resonant bandgap. If the two frequency ranges in Eqs. (26) and (27) overlap, the overlapping frequency range will not show a bandgap, but the two non-overlapping regions will correspond to two separate bandgaps. Finally, if the two frequency ranges are tuned to be adjacent or nearly adjacent, a single, wider bandgap will be created. Note that there is no benefit to having both negative dynamic mass and negative dynamic stiffness for the purpose of vibration reduction, as the two bandgaps effectively cancel each other. A typical structural response frequency response function (FRF) is shown in Fig. 2 for the two cases of distinct

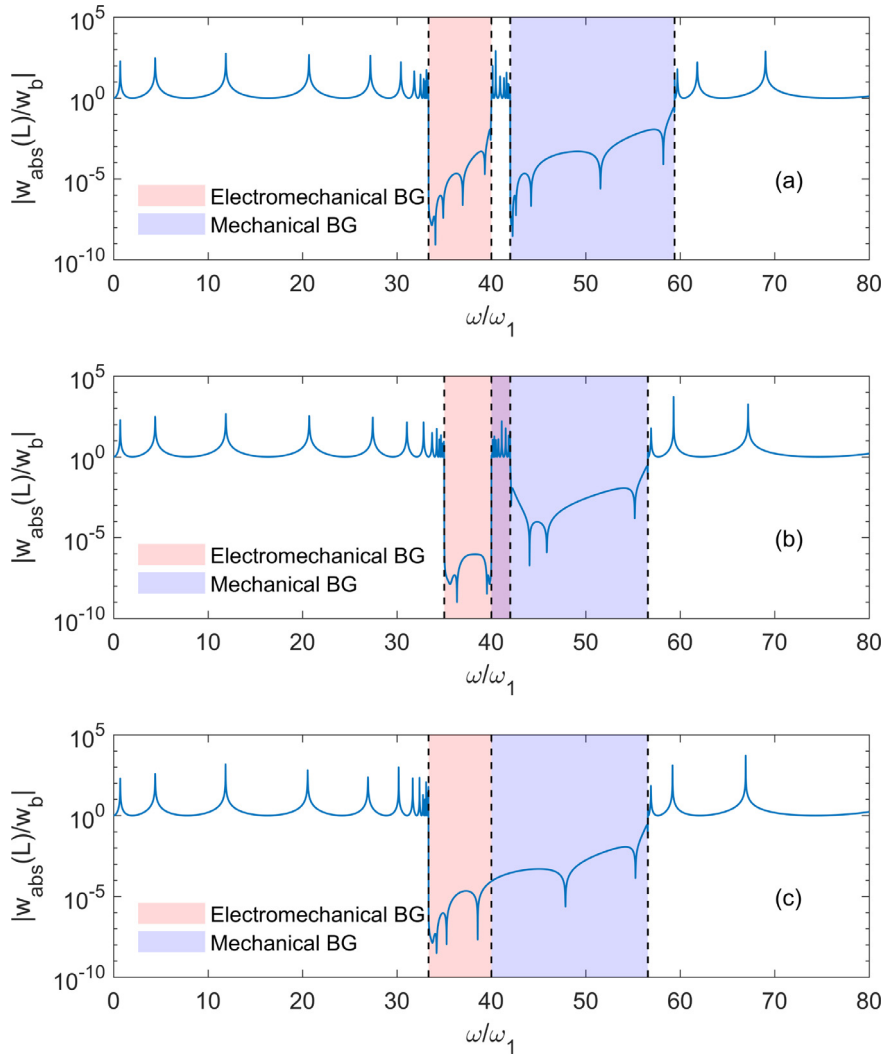


**Fig. 2.** Transmissibility frequency response function (tip motion per base motion) for a cantilever beam excited by base motion with  $\mu = 1$ ,  $\alpha = 0.44$ , and (a)  $\omega_e = 40\omega_1$ ,  $\omega_m = 42\omega_1$ , (b)  $\omega_e = 42\omega_1$ ,  $\omega_m = 40\omega_1$ , and (c)  $\omega_e = \omega_m = 40\omega_1$ . The dashed lines and shaded regions show the frequency ranges in Eqs. (26) and (27). In (a) the two frequency ranges are distinct, yielding two separate bandgaps. In (b) the two frequency ranges overlap, causing no bandgap to appear in the overlapping frequency range. In (c) the two frequency ranges are exactly adjacent, creating a single, wider bandgap.

bandgaps (i.e. Eqs. (26) and (27) distinct), overlapping bandgaps (i.e. Eqs. (26) and (27) overlapping), and combined bandgaps (i.e.  $\omega_e = \omega_m$ ).

It is theoretically possible to perfectly combine the two bandgaps by setting  $\omega_e = \omega_m$ , or alternatively  $\omega_m\sqrt{1+\mu} = \omega_e/\sqrt{1+\alpha}$ . The first of these two conditions is likely more feasible in a real system, where the system parameters  $\mu$  and  $\alpha$  may not be known precisely. Let  $\omega_e = \omega_m = \omega_t$  be the targeted frequency of the combined locally resonant bandgap. The bandgap edge frequencies can be obtained easily as

$$\frac{\omega_t}{\sqrt{1+\alpha}} < \omega < \omega_t\sqrt{1+\mu} \quad (28)$$

A simple way to visualize the response of the beam is to consider a harmonic point force excitation at the input location  $x_{in}$ , such that  $Q_r(j\omega) = F_0\phi_r(x_{in})$ , and measure the transmissibility, defined as

$$TR(\omega) = \left| \frac{W(x_{out}, \omega)}{W(x_{in}, \omega)} \right| \quad (29)$$

For a particular output location (e.g.  $x_{out} = L$  for a cantilever beam), the resulting transmissibility can be plotted as a heatmap vs. the input location and excitation frequency, as shown in Fig. 3. With this type of visualization, the bandgap is clearly visible as a frequency range of dramatic vibration attenuation, especially for excitation near the clamped end of the cantilever.

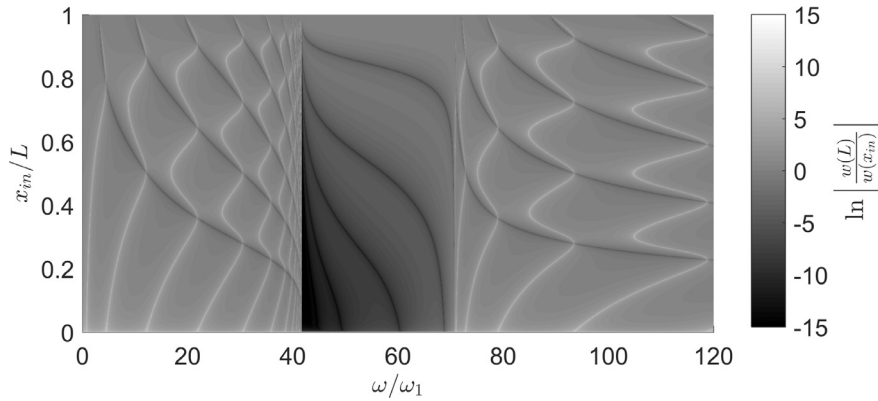


**Fig. 3.** Transmissibility (along the beam length) vs. normalized input excitation location  $x_m/L$  and normalized excitation frequency  $\omega/\omega_1$  with mass ratio  $\mu = 1$ , dimensionless electromechanical coupling term  $\alpha = 0.44$ , and target frequency  $\omega_t = 50\omega_1$ .

#### 4. Finite number of mechanical and electromechanical resonators

Clearly the approximations of Eqs. (19) and (20) require additional validation for systems with a finite number of segmented electrodes and resonators. For concreteness, we assume that the resonators and electrodes are placed evenly on a cantilever beam, such that  $x_j^L = (j-1)L/S$  and  $x_j^R = jL/S$ . For a particular set of values for  $\omega_t$ ,  $\alpha$ , and  $\mu$ , the approximate response of the beam to base excitation can be obtained using matrix inversion at each value of  $S$ , and the response can be plotted as a surface (or map) against  $S$  and the excitation frequency  $\omega$ . This is shown in Fig. 4 for a cantilever beam excited by base motion with  $\mu = 1$ ,  $\alpha = 0.44$ , and three different target frequencies  $\omega_t$ .

Fig. 4 contains significant information regarding the combination of the mechanical and electromechanical locally resonant bandgaps. For both mechanical and electromechanical components, the modeling and analysis framework given here for a finite structure captures the minimum number of unit cells required for bandgap formation. For all three considered target frequencies, both the mechanical bandgap (above the target frequency) and the electromechanical bandgap (below the target frequency) are clearly visible as frequency ranges of dramatic vibration attenuation. In all three figures, it is apparent that the mechanical bandgap appears for a smaller value of  $S$  (i.e. for less number of unit cells) than the electromechanical bandgap. This suggests that the approximation in Eq. (19) converges more quickly with increasing  $S$  than the approximation in Eq. (20). This follows from the mathematical intuition that the derivatives of the mode shapes of the structure will have larger slope, requiring more terms in the Riemann sum for convergence (i.e. more unit cells). Additionally, although with the assumption of an infinite number of mechanical and electromechanical resonators the two locally resonant bandgaps can be combined to form a single bandgap, it is clear from Fig. 4 that the finite metastructure exhibits a small frequency range between the two bandgaps that contains many resonant frequencies. This transitory frequency range becomes small for large values of  $S$ , but never completely disappears. These intermediate resonant frequencies are significantly attenuated by the presence of damping in the system. This is demonstrated in Fig. 5 for the specific case of a cantilever beam with  $S = 8$  mechanical and electromechanical resonators with  $\omega_e = \omega_m = 50\omega_1$ , as in the case of Fig. 4b, by comparing a completely undamped structure to a structure with viscously damped mechanical resonators that have 1% and 2% damping ratios (which are realistic values for composite devices and structures made from piezoelectric materials). Therefore, even for lightly damped resonators, the intermediate resonances within the combined bandgap are suppressed; hence the two bandgaps are expected to merge in real-world structures that have damping. It is worth mentioning that the resonator damping has the added effect of attenuating high frequency modes that occur at frequencies higher than the mechanical locally resonant bandgap, which is discussed in more detail in Hussein and Frazier (2012).

#### 5. Dispersion analysis using the plane wave expansion method

A commonly used technique to analyze locally resonant metamaterials is the plane wave expansion (PWE) method. A thorough discussion of PWE is beyond the scope of this work, but there are several papers that demonstrate its use with phononic crystals and locally resonant metamaterial structures (Laude, 2015; Xiao et al., 2013). Briefly, PWE assumes an infinite structure made from a repeated unit cell (i.e. lattice), and an expansion using complex exponentials is used for the displacement of the beam. Using the periodicity of the unit cell, an eigenvalue problem is obtained, which must be solved for all of the eigenfrequencies  $\omega$  at each Bloch wavevector in the irreducible region of the first Brillouin zone corresponding to the lattice of the structure. For this system, we consider a unit cell consisting of a piezoelectric bimorph with a mechanical resonator attached at the right edge of the unit cell. It can be shown that the resulting eigenvalue problem for the hybrid

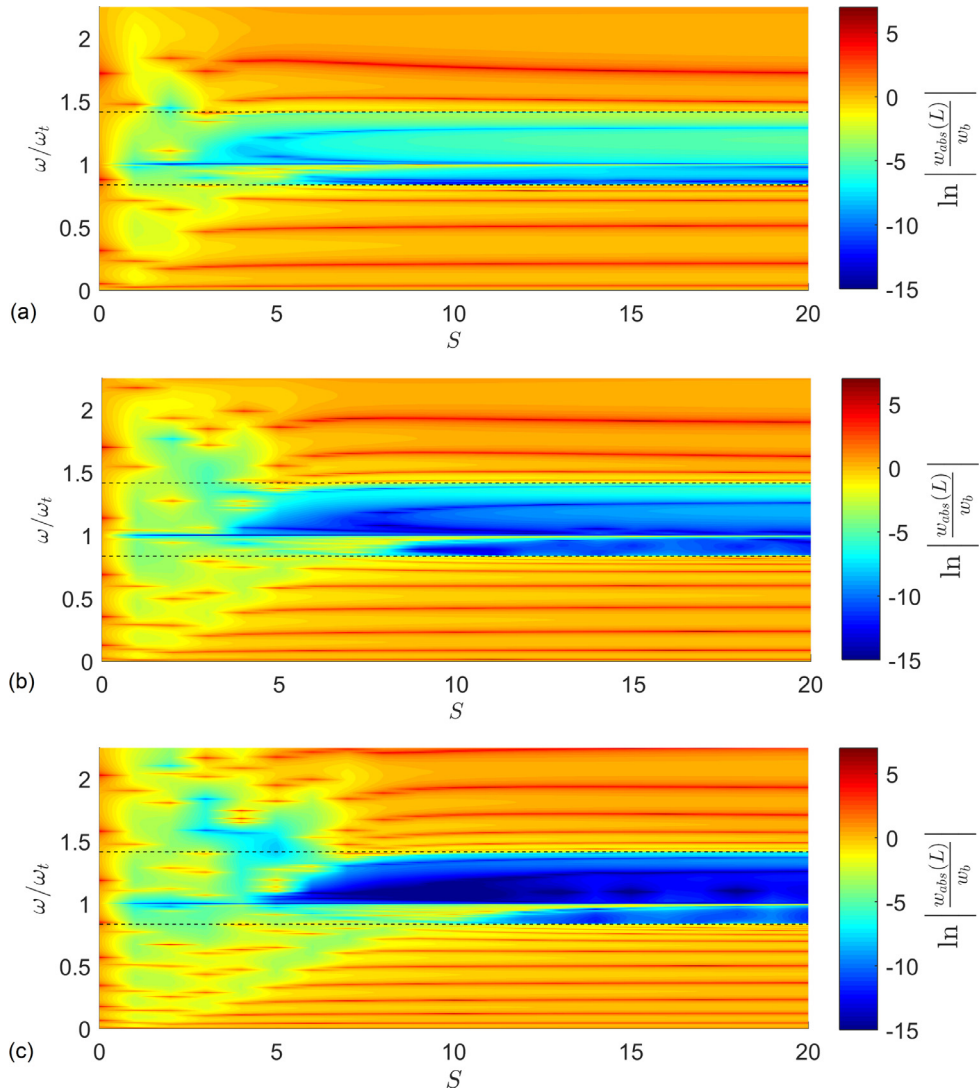


**Fig. 4.** Cantilever tip response vs. normalized excitation frequency  $\omega/\omega_t$  and number of segmented electrodes and resonators  $S$  with mass ratio  $\mu = 1$ , dimensionless electromechanical coupling term  $\alpha = 0.44$ , and target frequency  $\omega_e = \omega_m = \omega_t$  (a)  $\omega_t/\omega_1 = 20$ , (b)  $\omega_t/\omega_1 = 50$ , (c)  $\omega_t/\omega_1 = 100$ . Dashed lines show the bandgap edge frequencies predicted by Eq. (28).

mechanical-electromechanical locally resonant unit cell structure is

$$(EI(k + G_n)^4 - m\omega^2)W(G_n) - \frac{\vartheta}{L}v_0i(k + G_n)(1 - e^{-ikL}) - \frac{k_j}{L}\left(u_0 - \sum_n W(G_n)\right) = 0 \quad (30)$$

$$\omega_m^2\left(u_0 - \sum_n W(G_n)\right) - \omega^2u_0 = 0 \quad (31)$$

$$(\omega_e^2 - \omega^2)v_0 + i\frac{\omega^2\vartheta}{C_p}(1 - e^{ikL})\sum_n W(G_n)(k + G_n) = 0 \quad (32)$$

where here  $L$  is the length of the unit cell,  $u_0$  and  $v_0$  are the absolute resonator displacement and electrode voltage at the 0th unit cell,  $k$  is the Bloch wavevector (a scalar for the 1D problem),  $G_n$  is a reciprocal lattice vector, given by

$$G_n = \frac{2\pi n}{L}, \quad n \in \mathbb{Z} \quad (33)$$

$W(G_n)$  is the plane wave amplitude associated with the reciprocal lattice vector  $G_n$ , and  $C_p$  is the effective piezoelectric capacitance between the electrodes of the unit cell. This eigenvalue problem can be solved for the dispersion characteristics

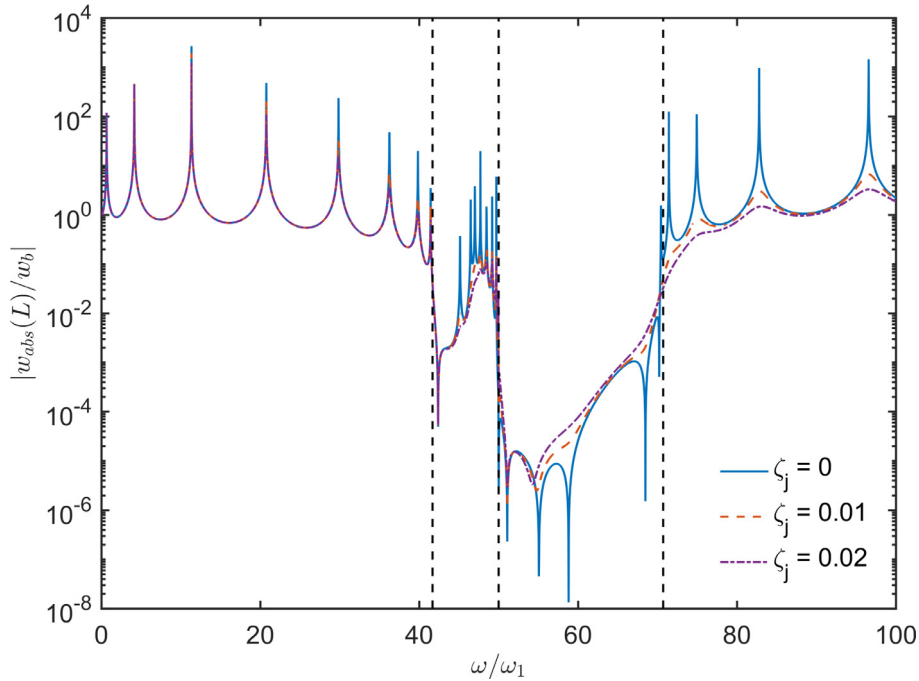


**Fig. 5.** Cantilever tip response vs. normalized excitation frequency  $\omega/\omega_1$  for  $S = 8$  mechanical and electromechanical resonators with mass ratio  $\mu = 1$ , dimensionless electromechanical coupling term  $\alpha = 0.44$ , and target frequency  $\omega_e = \omega_m = 50\omega_1$ . The solid line shows a completely undamped structure, the dashed line shows a structure whose mechanical resonators have 1% damping ratio, and the dash-dotted line shows a structure whose mechanical resonators have 2% damping ratio. Vertical dashed lines show the bandgap edge frequencies predicted by Eq. (28).

of the infinite structure. A set of results analogous to Fig. 2 showing distinct, overlapping, and merged bandgaps is shown in Fig. 6.

Clearly the bandgaps predicted by the frequency ranges in Eqs. (26) and (27) closely match the bandgaps predicted by the PWE dispersion analysis. Interestingly, in the case of overlapping bandgaps (Fig. 6b), the dispersion curve shows that modes in the negative-mass negative-stiffness frequency range display negative group velocity (negative slope in the dispersion curve). Additionally, even in the merged bandgap case (Fig. 6c), it is clear that there is a narrow frequency range where modes exist in between the two bandgaps. This transition region becomes narrower as the size of the unit cell becomes small relative to the first Bragg wavelength. These conclusions agree well with those obtained using modal analysis, validating both sets of results. It is important to note that PWE method does not provide the information of the number of unit cells required for bandgap formation, or other effects pertaining to the finite nature of the structure with specified boundary conditions, unlike the modeling and analysis framework presented in this work.

## 6. Conclusions

Locally resonant metastructures are finite structures exploiting locally resonant metamaterial concepts for low-frequency vibration attenuation as a result of bandgap formation for wavelengths much larger than the lattice parameter. In this work, we presented and analyzed a new class of locally resonant metastructures, namely hybrid mechanical-electromechanical metastructures. These hybrid metastructures made from piezoelectric laminates with segmented electrode pairs and attached mechanical resonators can simultaneously exhibit dynamic mass-based and stiffness-based locally resonant bandgaps. Under the assumption of a large number of mechanical and electromechanical resonators, the effective dynamic mass and dynamic stiffness of every mode becomes the same, as we obtained in closed form. Mechanical resonators create the possibility for negative dynamic mass over a limited frequency range, yielding the mechanical locally resonant bandgap, while the segmented electrodes and resonant shunt circuits create the possibility for negative dynamic stiffness over a limited frequency range, yielding the electromechanical locally resonant bandgap. When these two frequency ranges are distinct, two distinct bandgaps can be created. If the two frequency ranges overlap, there can be no bandgap in that overlapping frequency range, but two separate bandgaps are obtained in the non-overlapping ranges. Finally, if the two frequency ranges are placed adjacent to each other, a combined mechanical-electromechanical locally resonant bandgap can be created.

For a finite number of resonators and in the absence of damping, it was observed that the two bandgaps can never be completely combined in a seamless way, always leaving a narrowband frequency range between the two bandgaps that exhibits resonance. However, even for light damping in the resonators (for typical damping ratio values observed in linear vibration of piezoelectric-based composite devices and structures), the intermediate resonances forming within the bandgap

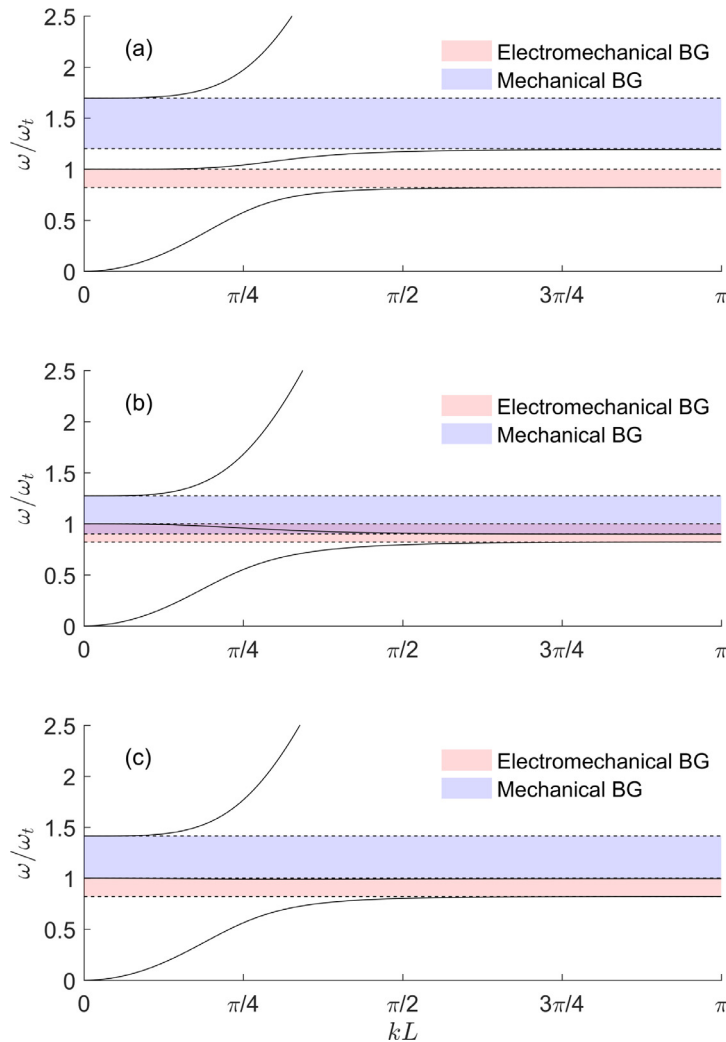


**Fig. 6.** Dispersion curves from plane wave expansion analysis for  $\mu = 1$ ,  $\alpha = 0.44$ ,  $f_t = \omega_t/2\pi = 500\text{Hz}$ ,  $l = 0.25\lambda_{\text{bragg}}$ , and (a)  $\omega_e = \omega_t$ ,  $\omega_m = 1.2\omega_t$ , (b)  $\omega_e = \omega_t$ ,  $\omega_m = 0.9\omega_t$ , and (c)  $\omega_e = \omega_m = \omega_t$ . The dashed lines and shaded regions show the frequency ranges in Eqs. (26) and (27). In (a) the two frequency ranges are distinct, yielding two separate bandgaps. In (b) the two frequency ranges overlap, causing no bandgap to appear in the overlapping frequency range. In (c) the two frequency ranges are exactly adjacent, creating a single, wider bandgap.

become insignificant, suggesting that the concept of merging the two bandgaps is feasible in real-world structures with damping. Ultimately, these hybrid locally resonant metastructures enable increased flexibility in the design of locally resonant bandgaps for low-frequency vibration attenuation in structures. Furthermore, there is the potential for other shunt circuits to be used in tandem with the mechanical resonators, such as for energy harvesting.

The overall concept of combining mechanical and electromechanical bandgaps in the same single metastructure can be leveraged in more complex topologies of metamaterial-based solids and structures, since the underlying principle and approach would be the same. That is, the mechanical and the electromechanical locally resonant bandgaps of piezoelectric-based structures will always form right above and below the identical target frequency of the mechanical and electromechanical resonators, respectively, yielding an enhanced bandgap as compared that obtained by purely mechanical or purely electromechanical counterparts separately. In addition to capturing the resulting wider bandgap, the modeling and analysis framework presented here accommodates the finite nature of the structure with specified boundary conditions (unlike standard unit cell analysis procedures, such as the plane wave expansion method), enabling the possibility of identifying the mode shape effects and the number of resonators required for bandgap formation, among others.

### Acknowledgment

This work was supported by the [Air Force Office of Scientific Research](#) grant [FA9550-15-1-0397](#) “Integrated multi-field resonant metamaterials for extreme, low frequency damping.”

## References

- Airoldi, L., Ruzzene, M., 2011. Design of tunable acoustic metamaterials through periodic arrays of resonant shunted piezos. *New J. Phys.* 13, 113010.
- Baravelli, E., Ruzzene, M., 2013. Internally resonating lattices for bandgap generation and low-frequency vibration control. *J. Sound Vib.* 332, 6562–6579.
- Bergamini, A.E., Zundel, M., Parra, E.A.F., Delpero, T., Ruzzene, M., Ermanni, P., 2015. Hybrid dispersive media with controllable wave propagation: a new take on smart materials. *J. Appl. Phys.* 118 (15), 154310.
- Casadei, F., Ruzzene, M., Dozio, L., Cunefare, K.A., 2010. Broadband vibration control through periodic arrays of resonant shunts: experimental investigation on plates. *Smart Mater. Struct.* 19, 015002.
- Chen, Y., Hu, G., Huang, G., 2017. A hybrid elastic metamaterial with negative mass density and tunable bending stiffness. *J. Mech. Phys. Solids* 105, 179–185.
- Dong, H.-W., Zhao, S.-D., Wang, Y.-S., Zhang, C., 2017. Topology optimization of anisotropic broadband double-negative elastic metamaterials. *J. Mech. Phys. Solids* 105, 54–80.
- Hagood, N.W., von Flotow, A., 1991. Damping of structural vibrations with piezoelectric materials and passive electrical networks. *J. Sound Vib.* 146 (2), 242–268.
- Hussein, M.I., Frazier, M.J., 2012. Metadamping: an emergent phenomenon in dissipative metamaterials. *J. Sound Vib.* 332, 4767–4774.
- Jin, Y., Bonello, B., Pan, Y., 2014. Acoustic metamaterials with piezoelectric resonant structures. *J. Phys. D Appl. Phys.* 47, 245301.
- Krushynska, A.O., Kouznetsova, V.G., Geers, M.G.D., 2014. Towards optimal design of locally resonant acoustic metamaterials. *J. Mech. Phys. Solids* 71, 170–196.
- Laude, V., 2015. *Phononic Crystals*. De Gruyter Studies in Mathematical Physics, Vol. 26. Walter de Gruyter GmbH, Berlin, Germany.
- Lesieutre, G.A., 1998. Vibration damping and control using shunted piezoelectric materials. *Shock Vib. Dig.* 30 (3), 187–195.
- Liu, Y., Su, X., Sun, C.T., 2015. Broadband elastic metamaterial with single negativity by mimicking lattice systems. *J. Mech. Phys. Solids* 74, 158–174.
- Liu, Z., Zhang, X., Mao, Y., Zhu, Y.Y., Yang, Z., Chan, C.T., Sheng, P., 2000. Locally resonant sonic materials. *Science* 289, 1734–1736.
- Matlack, K.H., Bauhofer, A., Krödel, S., Palermo, A., Daraio, C., 2016. Composite 3d-printed metastructures for low-frequency and broadband vibration absorption. *Proc. Natl. Acad. Sci.* 113 (30), 8386–8390.
- Nouh, M., Aldraihem, O., Baz, A., 2015. Wave propagation in metamaterial plates with periodic local resonances. *J. Sound Vib.* 341, 53–73.
- Oudich, M., Senesi, M., Assouar, M.B., Ruzzene, M., Sun, J.-H., Vincent, B., Hou, Z., Wu, T.-T., 2011. Experimental evidence of locally resonant sonic band gap in two-dimensional phononic stubbed plates. *Phys. Rev. B* 84, 165136.
- Senesi, M., Ruzzene, M., 2011. Piezoelectric superlattices as multi-field internally resonating metamaterials. *AIP Adv.* 1 (4), 041504.
- Sugino, C., Leadenham, S., Ruzzene, M., Erturk, A., 2016. On the mechanism of bandgap formation in locally resonant finite elastic metamaterials. *J. Appl. Phys.* 120 (13), 134501.
- Sugino, C., Leadenham, S., Ruzzene, M., Erturk, A., 2017a. An investigation of electroelastic bandgap formation in locally resonant piezoelectric metastructures. *Smart Mater. Struct.* 26 (5), 055029.
- Sugino, C., Xia, Y., Leadenham, S., Ruzzene, M., Erturk, A., 2017b. A general theory for bandgap estimation in locally resonant metastructures. *J. Sound Vib.* 406, 104–123.
- Wang, P., Casadei, F., Shan, S., Weaver, J.C., Bertoldi, K., 2014. Harnessing buckling to design tunable locally resonant acoustic metamaterials. *Phys. Rev. Lett.* 113, 014301.
- Xiao, Y., Wen, J., Yu, D., Wen, X., 2013. Flexural wave propagation in beams with periodically attached vibration absorbers: band-gap behavior and band formation mechanisms. *J. Sound Vib.* 332, 867–893.
- Yang, Z., Mei, J., Yang, M., Chan, N.H., Sheng, P., 2008. Membrane-type acoustic metamaterial with negative dynamic mass. *Phys. Rev. Lett.* 101 (20), 204301.
- Zhu, R., Liu, X.N., Hu, G.K., Sun, C.T., Huang, G.L., 2014. A chiral elastic metamaterial beam for broadband vibration suppression. *J. Sound Vib.* 333 (10), 2759–2773.